Continental Shelf Research 31 (2011) 685–694

Contents lists available at ScienceDirect

Continental Shelf Research

journal homepage: www.elsevier.com/locate/csr

Research papers

Response of salinity distribution around the Yellow River mouth to abrupt changes in river discharge

Yucheng Wang [a,1], Zhe Liu [a,b,*], Huiwang Gao [a], Lian Ju [c,d], Xinyu Guo [e]

[a] Key Laboratory of Marine Environment and Ecology (Ocean University of China), Ministry of Education, Qingdao 266100, China
[b] State Key Laboratory of Estuarine and Coastal Research, East China Normal University, Shanghai 200062, China
[c] Laboratory of Marine Spill Oil Identification and Damage Assessment Technology, the State Oceanic Administration, Qingdao 266033, China
[d] The Organization of North China Sea Monitoring Center, North China Sea Branch of the State Oceanic Administration, Qingdao 266033, China
[e] Center for Marine Environmental Studies, Ehime University, 2-5 Bunkyo-Cho, Matsuyama 790-8577, Japan

ARTICLE INFO

Article history:
Received 7 May 2010
Received in revised form
9 January 2011
Accepted 12 January 2011
Available online 19 January 2011

Keywords:
River plume
Discharge variation
Salinity distribution
Tidal mixing
Yellow River

ABSTRACT

To investigate how salinity changes with abrupt increases and decreases in river discharge, three surveys were conducted along six sections around the Yellow River mouth before, during and after a water regulation event during which the river discharge was increased from $\sim$200 to $>3000\ m^3\ s^{-1}$ for the first 3 days, was maintained at $>3000\ m^3\ s^{-1}$ for the next 9 days and was decreased to $<1000\ m^3\ s^{-1}$ for the final 4 days. The mean salinity in the Yellow River estuary area during the event varied $\sim$1.21, which is much larger than its seasonal variation ($\sim$0.50) and interannual variation ($\sim$0.05). Before the event, a small plume was observed near the river mouth. During the event, the plume extended over 24 km offshore in the surface layer in the direction of river water outflow. After the event, the plume diminished in size but remained larger than before the event. The downstream propagation of the plume (as in a Kelvin wave sense) was apparent in the bottom layer during the second survey and in both the surface and bottom layers during the third survey. The plume sizes predicted by the formulas from theoretical studies are larger than those we observed, indicating that factors neglected by theoretical studies such as the temporal variation in river discharge and vertical mixing in the sea could be very important for plume evolution. In addition to the horizontal variation of the plume, we also observed the penetration of freshwater from the surface layer into the bottom layer. A comparison of two vertical processes, wind mixing and tidal mixing, suggests that the impact of wind mixing may be comparable with that of tidal mixing in the area close to the river mouth and may be dominant over offshore areas. The change in Kelvin number indicates an alteration of plume dynamics due to the abrupt change in river discharge during the water regulation event.

© 2011 Elsevier Ltd. All rights reserved.

1. Introduction

River plumes are a general phenomenon in coastal water. They are affected by many factors, including the inertial effect at the river mouth, Coriolis force, winds (Fong, 1998; García Berdeal et al., 2002; Choi and Wilkin, 2007), ambient currents (Fong and Geyer, 2002; Xing and Davies, 2002), tidal currents (Isobe, 2005; Guo and Valle-Levinson, 2007), local topography (Kourafalou, 2001; Xing and Davies, 2002), stratification (Kourafalou, 1999; Wang et al., 2008) and river discharge (Pullen and Allen, 2000; Kourafalou, 2001; Yankovsky et al., 2001; Choi and Wilkin, 2007). The competition of these factors results in a variety of behaviors and time scales in river plumes.

Among the factors affecting river plumes, the river discharge and its temporal variation are particularly important. River discharge varies over many time scales. The longer time scales can be interannual or seasonal, whereas shorter time scales can last only several days, such as during a flood. Hereafter, we refer these short time scales as abrupt changes in river discharge.

Compared to the interannual or seasonal variations in river discharge, it is difficult to understand the influence of abrupt changes in river discharge on salinity distributions from field observations. Interannual and seasonal variation in salinity can be monitored by monthly or seasonal routine hydrographic surveys. However, the variation in salinity with an abrupt change in river discharge is difficult to capture with such routine surveys. In addition, an abrupt change in river discharge is often caused by a heavy precipitation event accompanied by bad weather conditions. The strong winds that coincide with bad weather conditions

* Corresponding author at: Key Laboratory of Marine Environment and Ecology (Ocean University of China), Ministry of Education, Qingdao 266100, China. Tel.: +86 532 66786568; fax: +86 532 66782810.
E-mail address: zliu@ouc.edu.cn (Z. Liu).
[1] Present address: Center for Marine Environmental Studies, Ehime University, 2-5 Bunkyo-Cho, Matsuyama 790-8577, Japan.

0278-4343/$ - see front matter © 2011 Elsevier Ltd. All rights reserved.
doi:10.1016/j.csr.2011.01.005

not only limit a field survey but also strongly affect the evolution of a plume.

The Yellow River (see Fig. 1 for the position) is one of largest rivers in the eastern Asian marginal seas. During the past several decades, its annual discharge has decreased gradually, partly due to climate change and partly due to human use (Wang et al., 2006), resulting in an unbalanced relationship between water and sediment inside the river and an increase in the salinity of the Bohai Sea (Wu et al., 2004). During 2002–2004, the Yellow River Conservancy Commission (YRCC) carried out a series of water regulation experiments to reshape the coordinative relationship between water and sediment by artificially releasing a large amount of water in a short time. Usually, a water regulation event last for only two weeks but the river discharge during the event accounted for greater than 20% of the annual discharge. Since 2005, water regulation events have been conducted regularly at the beginning of every flood season.

The salinity around the Yellow River mouth is expected to change dramatically with a large river discharge during a water regulation event, but the changes have not been well documented. With an interest in sediment transport, Wang et al. (2005) have reported that the plume near the river mouth containing high sediment moved rapidly during the water regulation event in 2005. Using a numerical model, Mao et al. (2008) have suggested that the variations in Yellow River runoff, including runoff during water regulation events, are important to the salinity not only in the area around the river mouth but also in the entire Bohai Sea. Based on a box model, Zhao et al. (2010) have examined the effects of water regulation events on the mean salinity of the Laizhou Bay, a semi-enclosed bay located southwest of the river mouth (see Fig. 1 for its position).

Treating the water regulation event as an opportunity to observe the response of a plume to an abrupt increase and decrease in river discharge, we carried out three surveys and measured the salinity and temperature around the Yellow River mouth before, during and after the water regulation event in 2009. After describing our observations in Section 2, we report the salinity distributions from our three surveys in Section 3 and discuss them in Section 4. Our conclusions are presented in Section 5.

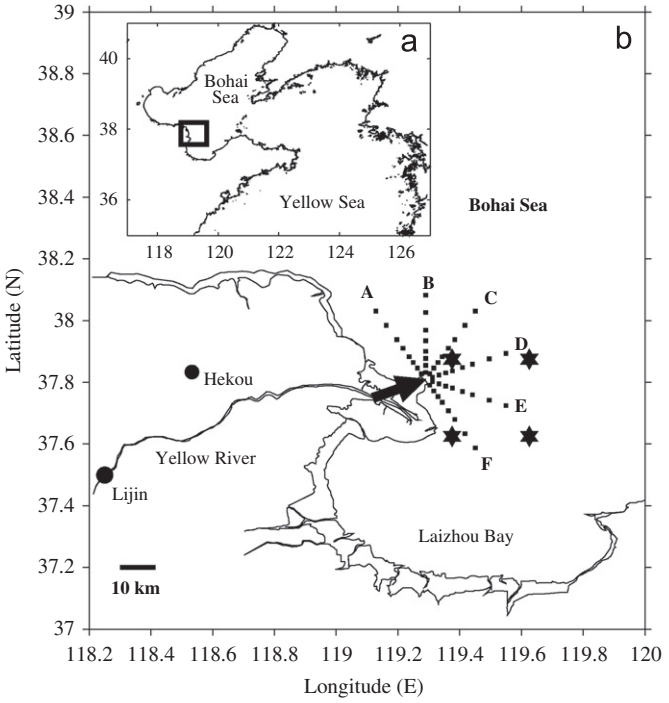

Fig. 1. (a) Location of the survey area and (b) the positions of the six sections, represented by characters A–F. The arrow denotes the outflow direction of the Yellow River water. Squares denote stations for salinity and water temperature measurements. Stars denote grid points for wind data from QuikSCAT.

2. Field observations

For the water regulation event of the Yellow River in summer of 2009, the river runoff recorded at Station Lijin (see Fig. 1b for its position), the nearest hydrological station to the river mouth (~100 km away), increased from 230 $m^3 s^{-1}$ on June 22 to 3170 $m^3 s^{-1}$ on June 24. After a runoff larger than 3000 $m^3 s^{-1}$ was maintained for 9 days, the runoff decreased from 3135 $m^3 s^{-1}$ on July 3 to less than 1000 $m^3 s^{-1}$ on July 7 (Fig. 2). Corresponding with the variation in river discharge, we carried out three surveys on June 19, July 1 and July 19, which were before, during and after the water regulation event, respectively (Fig. 2). The distance between Lijin Station and the Yellow River mouth may have caused a time lag of ~10 h between the record of river discharge and its arrival time at the Yellow River mouth during the water regulation event. Because our goal was to observe the subtidal movement of the plume, this time lag was neglected.

Six sections were arranged over a semicircle centered at the river mouth. Each section consisted of eight stations (Fig. 1) that were relatively denser near the river mouth. Three fishing boats were employed, with each covering two sections. The boats started at the same time and finished all the sections within ~10 h. The water temperature and salinity were measured by conductivity–temperature–depth profilers (CTDs).

A large amount of river sediment always flows into the sea during a regulation event and causes a change in bathymetry around the river mouth (Wang et al., 2005). We also found slight changes in water depth at some stations during our survey period. However, such changes in bathymetry had essentially no influence on the plume observations because the maximum difference in water depth was less than 10% of the whole depth.

In addition to the *in-situ* hydrographic data, daily satellite wind data from QuikSCAT Level 3 Daily, Gridded Ocean wind Vectors (see Fig. 1 for data positions; data were available from http://podaac.jpl.nasa.gov/DATA_PRODUCT/OVW/index.html#quikscat) and daily precipitation data observed at the Hekou weather station (see Fig. 1b for its position), which is the nearest weather station to the study area, were also used in this study.

3. Results

3.1. Variability in the horizontal distribution of salinity

The first survey was carried out on June 19, 2009, when the river discharge was low (173 $m^3 s^{-1}$). Before the water regulation event, low salinity water was concentrated in the northern region of the Yellow River mouth in only the surface layer (Fig. 3a). Because the salinity was relatively high, water with salinity lower than 26, which will be used to define the plume front in the second and third surveys, was rarely identified in the results of the first survey.

The second survey was on July 1, 2009, when the river discharge was high (3600 $m^3 s^{-1}$) and a high river discharge had been maintained for several days (Fig. 2). During the water regulation event, the surface salinity at most of the stations decreased dramatically, and low salinity water spread offshore far from the river mouth (Fig. 3d). The low salinity water in the

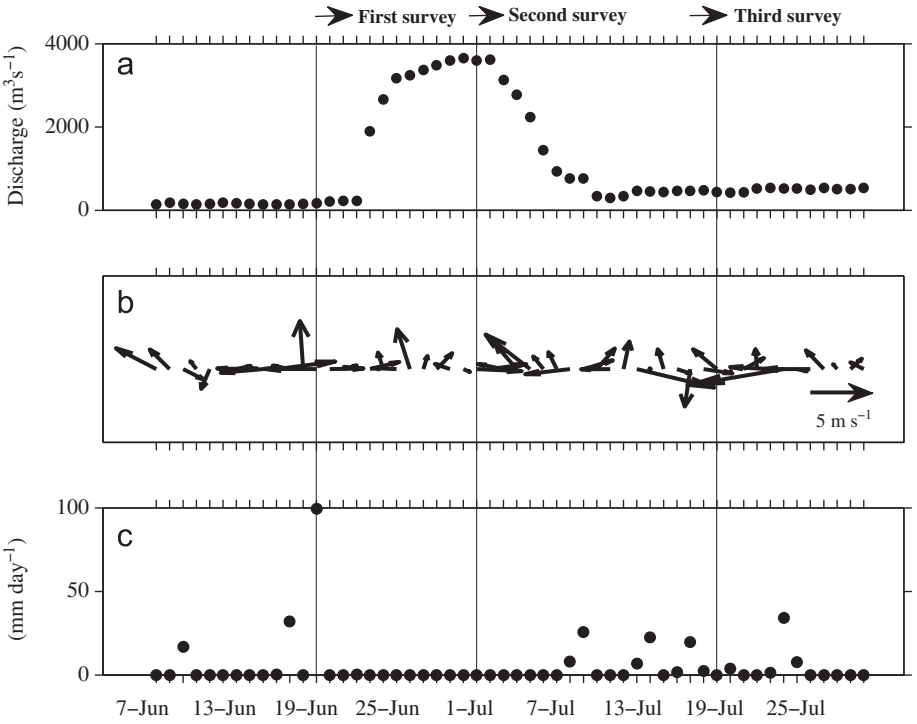

Fig. 2. (a) Daily discharge of the Yellow River, (b) daily sea surface winds and (c) daily precipitation rate from June 7 to July 30, 2009. The three vertical bars indicate the dates of the three surveys. The daily discharge was recorded at Station Lijin; the wind data is the average of the four QuikSCAT grid points; daily precipitation was observed at the Hekou weather station. The positions of Station Lijin, the four QuikSCAT grid points and the Hekou weather station are given in Fig. 1.

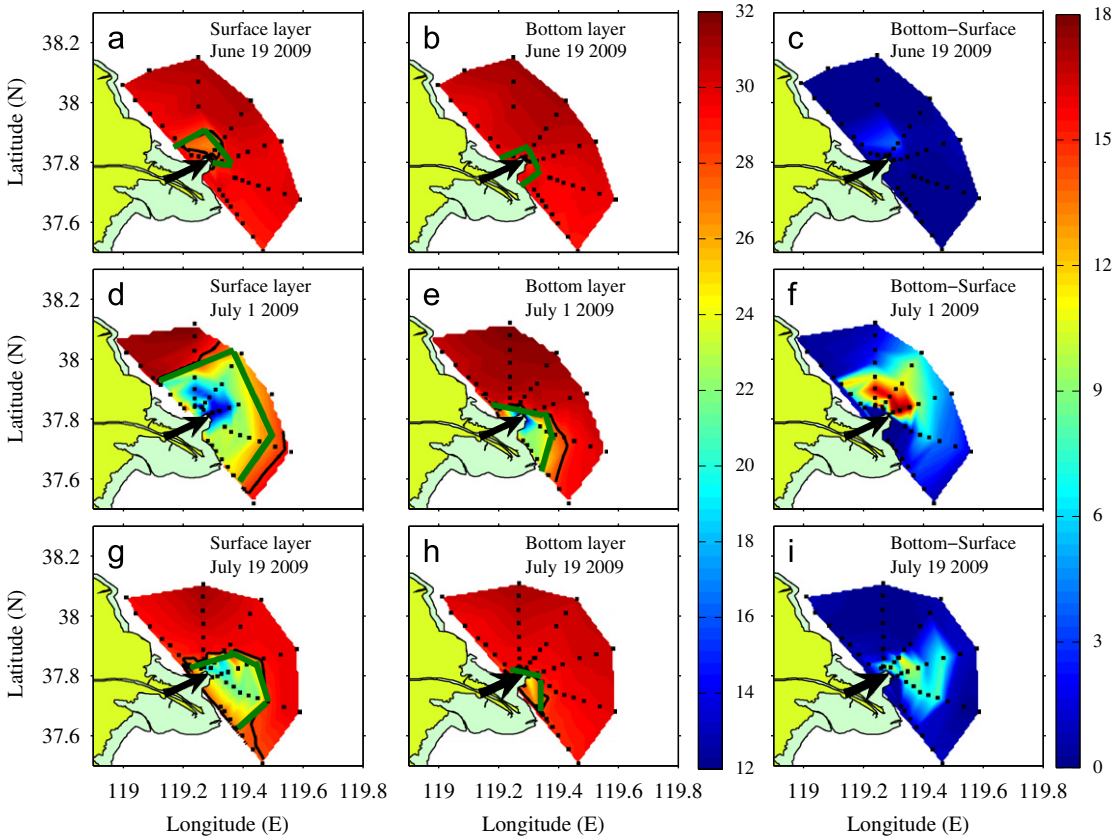

Fig. 3. Horizontal distribution of salinity in the surface layer (0–1 m below the sea surface), in the bottom layer (1 m above the sea bottom) and their difference (bottom layer – surface layer) in the first survey ((a)–(c)), second survey ((d)–(f)) and third survey ((g)–(i)). Black bold lines denote the 28-isohaline in the first survey and the 26-isohalines in the second and third surveys. Arrows denote the outflow direction of the Yellow River water. Squares denote CTD stations. The green bold line in each panel denotes the position of the maximum magnitude of the horizontal gradient in salinity.

surface layer was distributed symmetrically to the direction of river water outflow, while that in the bottom layer was mainly concentrated in the southern area of the river mouth (Fig. 3e), the downstream direction, in a Kelvin wave sense. Accordingly, a large vertical difference in salinity was found in the northeastern area of the river mouth (Fig. 3f). The minimum salinity in the second survey was 8.90 in the surface layer in the vicinity of the river mouth, and the largest salinity difference between the bottom and surface layers was 17.50 at the same station. Because the depth of this station was only 2.5 m, the outflow of freshwater from the river mouth was driven across a very thin surface layer.

The third survey was conducted on July 19, 2009, when the river discharge had decreased to 478 $m^3 s^{-1}$. After the water regulation event, the plume diminished in size (Fig. 3g and h) and the low salinity water in the surface layer had veered southward (Fig. 3g). This result indicated that the extension of the river plume depended strongly on the river discharge and the mixing of low salinity water within the plume with ambient water. In addition, the upwelling favorable winds before the second survey and the downwelling favorable winds before the third survey may also have contributed to the differences in the distribution of low salinity water (Fig. 3g).

The vertical salinity difference was small in the first survey (Fig. 3c), increased to its largest value during the second survey (Fig. 3f) and decreased rapidly in the third survey (Fig. 3i). The rapid reduction in vertical salinity difference between the second survey and the third survey reflects the influence of vertical mixing.

Practically, a plume front can be defined as a place with maximum horizontal gradient of a variable such as salinity or turbidity. Here, we calculated the horizontal gradient of salinity in each survey and the position of its maximum magnitude is shown in Fig. 3. The position of the maximum magnitude of the salinity gradient generally coincided with the 28-isohaline during the first survey and the 26-isohaline during the second and third surveys.

For a clear image of the plume front movement, we present the distribution of the 28-isohalines for the first survey and the 26-isohalines for the second and third surveys in the surface and bottom layers from three surveys in one figure (Fig. 4). According to the results, the plume front was barely identifiable before the water regulation event, spread out in the direction of river water outflow when the river discharge increased to a high value during the event and returned to the river mouth as the river discharge decreased after the event. During the evolution of the plume, the diluted water gradually flowed in the downstream direction in a Kelvin wave sense.

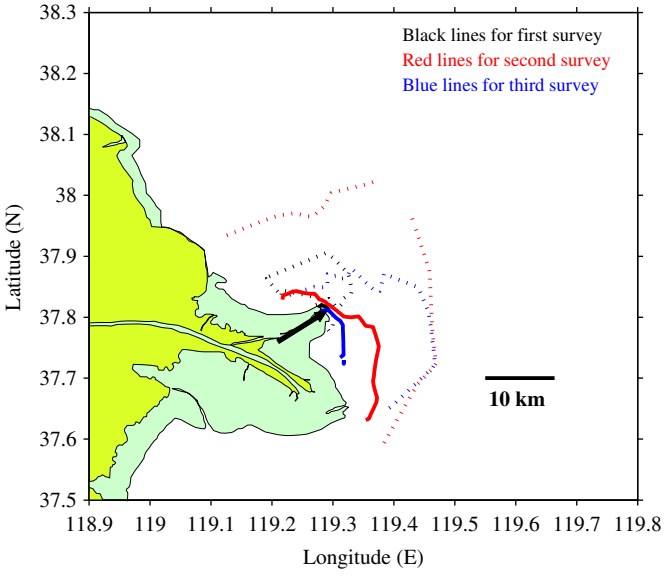

Fig. 4. Positions of the plume fronts in the surface layer and bottom layer observed during the three surveys. The plume front was defined as the location of the 28-isohaline in the first survey and the location of the 26-isohaline in the second and third surveys. Dashed lines represent the plume fronts in the surface layers, while solid lines are the plume fronts in the bottom layers.

The factors affecting the movement of a plume competed with each other during the water regulation event. As a buoyancy-driven current, the Yellow River plume tends to move southward, a downstream direction in a Kelvin wave sense. According to Wang et al. (2008), the inherent northward tidally induced residual current in our study area tends to prevent the plume from extending southward. When the river discharge was small as in the first survey, the buoyancy-driven current was weak and the low salinity water was limited to the upstream area by the tidally induced residual current. With input of a large amount of freshwater, as before and during the second survey, the influence of the tidally induced residual current became relatively small and the inertial effect of river water led the low salinity water to distribute itself in a quasi-symmetric structure in the direction of river water outflow. In addition, the upwelling favorable winds between the first and second surveys helped the plume spread offshore. The development of the buoyancy-driven current between the second and third surveys and the downwelling favorable winds prior to the third survey may have been responsible for the low salinity water observed in the downstream area in the third survey.

In order to quantitatively examine the temporal change of salinity, the daily rate of variation of salinity in the surface and bottom layers was calculated from the results of three surveys (Fig. 5). During the period from the first survey to the second survey, the mean reduction rate of salinity was maximal near the river mouth (-1 day^{-1}) in the surface layer and decreased with distance from the river mouth (Fig. 5a). It was much lower in the bottom layer than in the surface layer (Fig. 5b). During the period from the second survey to the third survey, the surface salinity increased with a maximum rate of 0.5 day^{-1} in the northern area of the river mouth (Fig. 5c). The bottom salinity increased on the downstream side but decreased on the upstream side (Fig. 5d). The surface salinity at the northwestern corner of the survey area increased during the period from the first survey to the second survey (Fig. 5a), but decreased during the period from the second survey to the third survey (Fig. 5c), indicating a time lag in the spread of freshwater toward the upstream area.

3.2. *Variability in the vertical distribution of salinity*

The salinity observed in the first survey was relatively uniform vertically (left panels in Fig. 6). Low salinity (<28) appeared only in the surface layer of Section C. Some stations near the river mouth along Section B that were also expected to have low salinity were not observed due to the bad weather conditions.

The salinity decreased in the second survey at all sections, but the thickness of the low salinity water layer was different among sections (middle panels in Fig. 6). With the input of a large amount of freshwater, low salinity water was observed in the surface layer. Accordingly, the position of the 30-isohaline became deeper at all sections except for Section A, indicating the possibility of onshore movement of high salinity water there. The low salinity water was separated from the bottom water at Sections A–D but remained in contact with the bottom water at Sections E and F.

After the reduction in river discharge, in the third survey, the diluted water stayed close to the river mouth and remained in the surface layer (right panels in Fig. 6). The salinity of the bottom

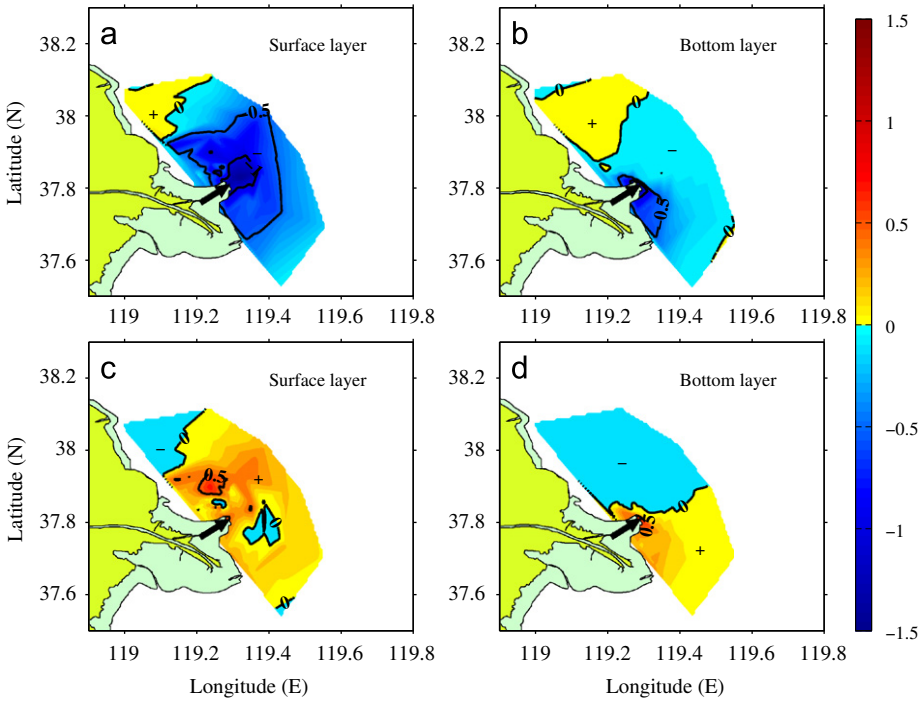

Fig. 5. Rates of temporal variation of (a) surface salinity between the second and first surveys, (b) bottom salinity between the second and first surveys, (c) surface salinity between the third and second surveys and (d) bottom salinity between the third and second surveys. The symbol '+' denotes an increase in salinity, while that of '−' a decrease in salinity. The unit is day^{-1}.

water decreased at Sections A–D but increased at Sections E and F. Because horizontal mixing with ambient salty water may increase the salinity of bottom water and the horizontal spreading of low salinity bottom water could be limited by strong tidal currents, the decrease in bottom water salinity can be explained by freshwater supply via vertical mixing from the surface layer during the period between the second survey and the third survey. On the other hand, the increase in bottom water salinity was likely caused by the onshore intrusion of high salinity ambient water from outside the survey area because the increase occurred along only two sections.

Until now, we have presented how the abrupt increase or decrease in river discharge affected the salinity distribution in the horizontal and vertical directions. We have not shown any results on variations in water temperature because river discharge has little influence on water temperature. However, it has been reported that the offshore movement of a plume depends on the density stratification due to water temperature (Wang et al., 2008). It is, therefore, necessary to examine how the density stratification depends on water temperature and salinity and whether this relationship changes with river discharge.

We adopted the following method to examine the contribution of water temperature and salinity to stratification defined by the density difference (D) between the surface layer and the bottom layer. The temperature was fixed to that of the bottom layer and we used the observed salinity to calculate the density difference (DS) between the surface layer and the bottom layer. We also fixed salinity to that of the bottom layer and used the observed temperature to calculate the density difference (DT) between the surface layer and the bottom layers. As first-order approximations, DS/D and DT/D are considered to be the density stratification due to salinity and temperature, respectively.

In general, both temperature and salinity contributed to stratification (Fig. 7a and b). The contribution from salinity decreased apparently with distance from the river mouth. For example, the salinity contributed 70% to the density stratification at onshore stations (Fig. 7a), but less than 50% at offshore stations. Furthermore, the linear regressions of DS/D and DT/D to the distance from the river mouth indicate that the contribution of salinity to stratification is proportional to the river discharge (Fig. 7a), whereas that of temperature to stratification is inversely proportional to the river discharge (Fig. 7b).

Because the river plume tends to turn right after entering the sea, the influence of salinity on density stratification probably depends on the relative position of the measurement station in relation to the plume. In order to examine this possibility, the study area was divided into three subregions: an upstream region (Sections A and B), an outflow region (Sections C and D) and a downstream region (Sections E and F). The proportional relationship between the contribution of salinity to density stratification and the river discharge was generally kept in the three subregions, except for in the upstream region during the first and third surveys (Fig. 7c). Among the possible causes for this exception (that the contribution of salinity to density stratification is larger in the first survey than in the third survey), the fast movement of the river plume from the upstream and outflow regions to the downstream region after the large river discharge before and during the second survey and subsequent intrusion of ambient water into the upstream region must be an important process.

3.3. Variability of water exchange capability

To determine the variation in the water exchange capability of the waters around the Yellow River mouth during our survey period, we computed the flushing time (τ), which is defined as the ratio of the volume (VOL) of the target region and the inflow flux (V_{in}) of seawater from outside the target region (Sheldon and Alber, 2006). The target region here was set as the survey area, which had a volume of 1.65×10^{10} m^3.

In order to obtain the inflow flux V_{in}, a simple box model was configured based on the conservation of volume and salt within

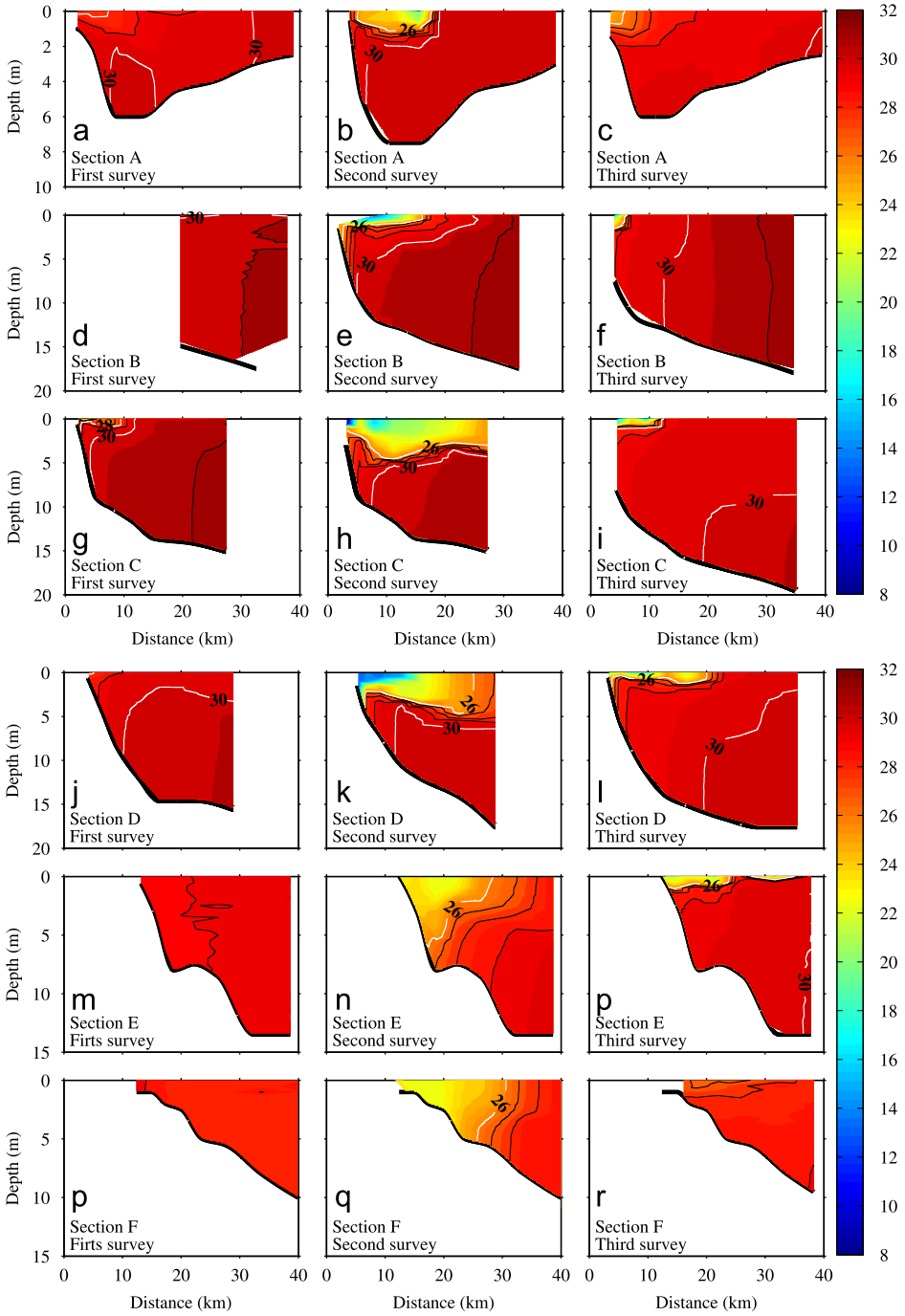

Fig. 6. Vertical distributions of salinity observed for three surveys along Section A (a–c), Section B (d–f), Section C (g–i), Section D (g–l), Section E (m–o) and Section F (p–r). The white lines denote the 26-isohaline, 28-isohaline and 30-isohaline.

the box (Gordon et al., 1996):

$$V_{out} = V_Q + V_{in} + P - E \tag{1}$$

$$VOL\frac{dS}{dt} = V_{in}S_0 - V_{out}S \tag{2}$$

Here, V_{out} is the outflow flux from the survey area, V_Q is the river discharge, P and E are the precipitation and evaporation over the survey area, respectively, S is the spatially averaged salinity within the survey area and S_0 is the salinity outside the survey area. From Eqs. (1) and (2), V_{in} is obtained as follows:

$$V_{in} = \frac{1}{(S_0 - S)}\left((V_Q + P - E)S + VOL\frac{dS}{dt}\right) \tag{3}$$

We applied Eq. (3) to every two consecutive surveys. The value of S_0 was set to 31.60, the largest salinity observed during the three surveys. Denoting the survey times as T_1, T_2 and T_3 the spatially averaged salinity within the survey area as S_1, S_2 and S_3, respectively, we obtained S as $0.5(S_1+S_2)$ and $0.5(S_2+S_3)$, dS/dt as $(S_2-S_1)/(T_2-T_1)$ and $(S_3-S_2)/(T_3-T_2)$ for the period from the first survey to the second survey and that from the second survey to the third survey, respectively. The other variables V_Q, P and E were treated as the mean values between two subsequent surveys and calculated from observed daily data.

Before analyzing the box model results, we examined the relative role of surface freshwater flux in the river discharge. The average precipitation rate (6.02 mm day^{-1}) during the entire survey period

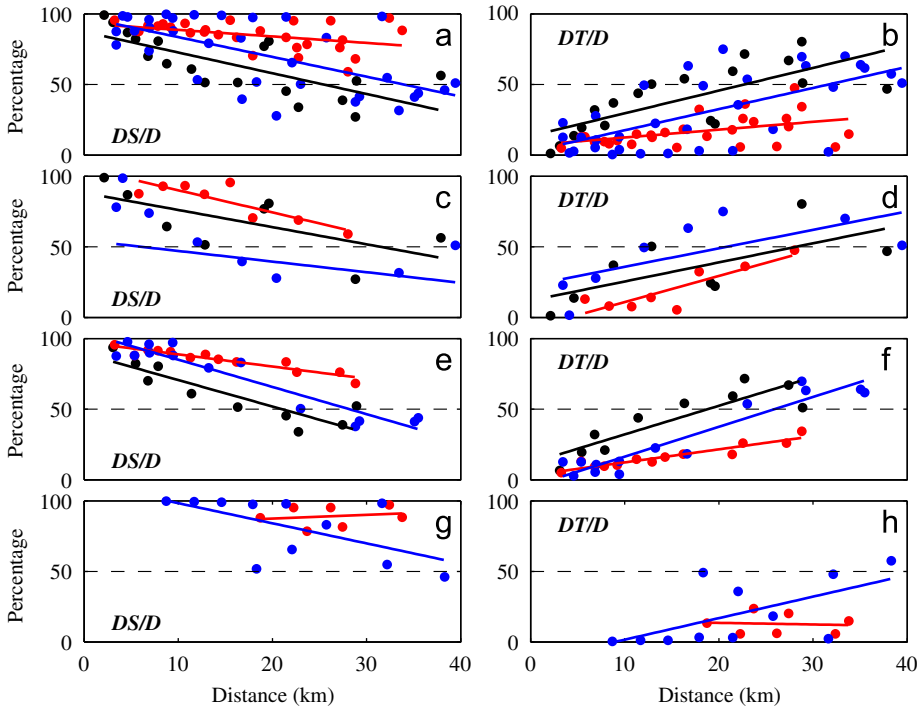

Fig. 7. Contributions of vertical variations in salinty (left panel) and water temperature (right panel) to density stratification at the stations where the density difference between the surface and bottom layers was larger than 1 kg m^{-3}. The dots were caculated from data observed for each survey, and the lines are based on first-order linear regressions. The black, red and blue colors for the dots and lines are for the first, second and third surveys, respectively. Panels (a) and (b) present data from all stations; (c) and (d) present data from Sections A and B; (e) and (f) present data from Sections C and D; and (g) and (f) present data from Sections E and F.

Table 1
Calculation of flushing time. See Eq. (3) for meaning of each term. dS/dt is in day^{-1}; V_Q, P, E, V_{in}, V_{out} are in 10^8 m^3 day^{-1} and τ is in days.

Period	S	S_0	dS/dt	V_Q	P	E	V_{in}	V_{out}	τ
First survey to second survey	30.11	31.60	−0.11	1.96	0.12	0.18	26.21	28.11	6.3
Second survey to third survey	28.90	31.60	0.05	0.95	0.07	0.13	12.58	13.48	13.1

was obtained from the daily observation data at the Hekou weather station. According to Yan (1999), the evaporation rate in our study area in the summer is less than 0.56 mm day^{-1}. Given the net surface freshwater flux (6.02–0.56=5.46 mm day^{-1}) and the surface area of the box (1.55×10^9 m^2), the surface freshwater flux was 8.5×10^6 m^3 day^{-1}, which is smaller than the Yellow River mean discharge (1.38×10^8 m^3 day^{-1}) from June 19 to July 19 by almost two orders of magnitude. Therefore, the surface freshwater flux contributed extremely little to the water volume budget and salt budget during the period of the water regulation event, although it could be important for the long-term variations in salinity in the study area (Wu et al., 2004). It must be noted that a direct estimation of evaporation rate using a bulk formula gave a different value from that of Yan (1999). However, using the direct estimate did not change the fact that the surface freshwater flux played a negligible role in the water volume budget. The calculated flushing time was 6.3 days for the period from the first survey to the second survey and 13.1 days for the period from the second survey to the third survey (Table 1). The difference in flushing time results from the difference in the inflow flux of seawater from outside the box, which was generally proportional to the river discharge with a ratio approximately 15. Therefore, increasing the river discharge generally promotes the water exchange of our target region.

An alternative method to calculate the variability in water exchange capability is to examine the freshwater budget inside the survey area. The volume of freshwater can be calculated by the following equation (Choi and Wilkin, 2007):

$$F_P = \int\int_{h_1}^{h_2} \frac{(S_0 - S_A)}{S_0} dzdA \tag{4}$$

Here, S_A denotes the observed salinity at each station, S_0 is the background salinity of 31.6, A is the surface area of the target region and h_1 and h_2 denote water depths. Because most low salinity water was observed in the surface layer, we separated the water column into two layers. The upper layer is from the surface to a depth of 5 m, while the lower layer extends from the 5 m depth to the sea bottom.

The calculated freshwater volumes in the upper layer were 4.12×10^8, 9.98×10^8 and 5.19×10^8 m^3, in the first, second and third surveys, respectively. The increase and decrease in the freshwater volume of the upper layer is consistent with the changes in river discharge. The calculated freshwater volumes in the lower layer were 3.64×10^8, 4.10×10^8 and 4.70×10^8 m^3, respectively. The increase in the freshwater volume of the lower layer between the second and third survey is not consistent with the change in river discharge, indicating the downward transport of freshwater via vertical mixing.

During the period between the first survey and the second survey, the freshwater volume within entire water column increased by 6.32×10^8 m^3, the majority of which (5.86×10^8 m^3) entered the upper layer, while the rest (0.46×10^8 m^3) entered the lower layer.

During the period from the second survey to the third survey, the freshwater volume within entire water column decreased by 4.19×10^8 m^3. The lower layer kept receiving freshwater (0.60×10^8 m^3), but the upper layer lost much more freshwater (4.79×10^8 m^3).

The freshwater input from the Yellow River into the box was 25.51×10^8 m^3 during the period between the first survey and the second survey and 17.14×10^8 m^3 during the period between the second survey and the third survey. Excluding the change in freshwater volume within the box, we know that 19.19×10^8 and 21.33×10^8 m^3 of freshwater flowed out of the box through its lateral boundary during the two periods mentioned above. Accordingly, the daily freshwater fluxes through the lateral boundary of the box were 1.48×10^8 and 1.19×10^8 m^3 day^{-1} during the two periods. The result that the first period had a larger freshwater flux through lateral boundary than the second period is consistent with the difference in flushing time. Therefore, the exchange rate between the area at the mouth of the Yellow River and the outside region becomes large with the abrupt increase in river discharge and becomes small with the abrupt decrease in river discharge.

4. Discussion

4.1. Tidal mixing and wind mixing

As presented in Section 3, vertical mixing is likely to be important to the salinity distribution. Both tidal mixing and wind mixing contribute to vertical mixing. Here, we compare their contributions.

We computed the stirring power of the tidal current (P_t) and that of the surface wind stress (P_w) using an empirical formula given by Simpson and Bowers (1981):

$$P_t=\frac{4}{3\pi}\varepsilon k_b\rho\frac{U^3}{h} \tag{5}$$

$$P_w=\delta k_s\rho_a\frac{W^3}{h} \tag{6}$$

In these equations, U is the amplitude of tidal current near the seabed, h is the typical depth of the area, W is the wind speed, ρ is the density of seawater (1020 kg m^{-3}), ρ_a is the density of air (1.3 kg m^{-3}), ε is the efficiency of tidal mixing (2×10^{-3}, according to Zhao et al., 1994), δ is the efficiency of wind mixing (0.11, according to Zhao et al., 1994), k_b is the effective drag coefficient for bottom stresses (1.2×10^{-3}, according to Zhao et al., 2001) and k_s is the effective drag coefficient for surface stresses (6.4×10^{-5}, according to Simpson and Bowers, 1981).

The amplitude of the observed tidal flow around the river mouth was approximately 1 m s^{-1} at a station with a water depth of 5 m (Wang et al., 2005), which gives a P_t of 2.1×10^{-4} W m^{-3}. Meanwhile, the daily P_w calculated based on the same water depth and the daily satellite wind speed during the period from June 19 to July 19 results in an average value of 3.2×10^{-4} W m^{-3}. Consequently, the tidal mixing was comparable with the wind mixing in this area. However, the magnitude of tidal currents and water depth change rapidly in space. For example, at a station far away from the river mouth, where the water depth is 15 m and the tidal flow was ~0.5 m s^{-1} (station A5 in Qiao et al., 2006), P_t becomes 0.9×10^{-5} W m^{-3}, which is smaller than the stirring power of wind (1.1×10^{-4} W m^{-3}) by almost an order. Therefore, although the tidal mixing and wind mixing are similar in strength in the area close to the Yellow River mouth, wind mixing is dominant over offshore areas. The sharper decrease in tidal mixing compared to wind mixing between onshore areas and offshore areas looks reasonable if we consider the spatial scales of wind velocities and tidal currents.

The above calculation has a large uncertainty because the data for tidal currents was not directly measured in our surveys. In addition, the mixing efficiency parameters ε and δ were also from other studies. If we use the mixing efficiency parameters $\varepsilon=4\times10^{-3}$ and $\delta=2.3\times10^{-2}$ from Simpson and Bowers (1981), P_t and P_w become 4.2×10^{-4} and 7.2×10^{-5} W m^{-3}, respectively, in onshore areas and 1.7×10^{-5} and 2.4×10^{-5} W m^{-3} in offshore areas. In this case, tidal mixing is dominant over onshore areas and is comparable with wind mixing over offshore areas. Therefore, we need to keep in mind the uncertainty of our conclusion based on the parameters given by Zhao et al. (1994) although those parameters are more suitable to our survey area than the parameters given by Simpson and Bowers (1981).

To confirm the effects of tidal mixing on the plume, we also need to compare the tidally induced bottom water boundary layer height with the water depth because low salinity water was usually only distributed in the surface layer, where tidal mixing may not reach.

The bottom boundary layer thickness caused by the clockwise component (B_-) and anticlockwise component (B_+) of tidal currents were calculated by the following equations (Prandle, 1982):

$$B_-=\left(\frac{2Nz}{(\omega-f)}\right)^{1/2} \tag{7}$$

$$B_+=\left(\frac{2Nz}{(\omega+f)}\right)^{1/2} \tag{8}$$

Here, ω is the frequency of the tidal constituent (M_2 tide, 1.4×10^{-4} s^{-1}), N_z is the eddy viscosity coefficient, and f is the Coriolis parameter (0.9×10^{-4} s^{-1}). The eddy viscosity coefficient is related to tidal current amplitude (U), water depth (h) and the effective bottom drag coefficient (k_b) by the following equation (Prandle, 1982), which may be applied to all of the areas where tidal currents are dominant:

$$N_z=\frac{1}{2}k_bUh \tag{9}$$

The tidal currents in our survey area are strong and the stratification is weak as observed before the water regulation event (Fig. 6). During or after the water regulation event, the stratification was concentrated in the surface layer and the water from the sea bottom was well mixed to a considerable height (Fig. 6). All these facts suggest that tidal mixing is an important engine for vertical mixing in our study area and that the usage of the empirical formula given by Prandle (1982) for eddy viscosity is a reasonable choice.

According to Liu (1989), the tidal currents around the Yellow River mouth are generally rectilinear, suggesting the same amplitude of the anticlockwise and clockwise components, which are the half of the amplitude of the tidal current. At the station near the river mouth (Wang et al., 2005), N_z is estimated to be 1.5×10^{-3} m^2 s^{-1}, yielding B_+ and B_- values of 4 and 8 m, respectively. At the station a little farther from the river mouth (Qiao et al., 2006), N_z is estimated to be 2.3×10^{-3} m^2 s^{-1}, yielding B_+ and B_- values of 4 and 10 m, respectively. Accordingly, tidal mixing can reach the sea surface in the former case but can only reach the middle layer in the latter case. Therefore, the combination of tidal mixing and wind mixing is important for the vertical transport of freshwater in the area far from the river mouth.

4.2. Offshore distance of the river plume

As depicted in Fig. 4, the offshore distance of the river plume changed distinctly in the surface layer and the bottom layer during the observation period. Before the water regulation event, the river

plume front defined by the 28-isohaline was hardly identifiable. During the water regulation event, the offshore distance of the river plume front in the surface layer was largest (>24 km) in the direction of river water outflow, while that of the bottom layer was largest (<10 km) in the downstream region. After the water regulation event, the largest offshore distance was $\sim$15 km in the surface layer and only $\sim$3 km in the bottom layer in the downstream region.

Yankovsky and Chapman (1997) classified plumes into three types: surface-advected plumes, bottom-advected plumes and intermediate plumes. According to the vertical structure of the plume observed around the Yellow River mouth, we classified it as a surface-advected plume.

The offshore distance of a surface-advected plume can be calculated by the following equation (Yankovsky and Chapman, 1997):

$$y_s = \frac{2(3g'h_i + v_i^2)}{(2g'h_i + v_i{}^2)^{1/2} f} \tag{10}$$

where y_s is the offshore distance of the plume, g' is the reduced gravity based on the inflow density anomaly, $g' = g(\Delta\rho/\rho)$ (g is the gravity acceleration, ρ is the density of ambient water and $\Delta\rho$ is the density difference between the river plume and the ambient water at the river mouth), h_i is the inflow depth and v_i is the inflow velocity.

Substituting the corresponding values from the three surveys into Eq. (10), the offshore distances of the plume front were calculated (Table 2). In general, the offshore distances of the observed plumes were shorter than those predicted by Eq. (10). For example, the observed plume fronts in the second and third surveys were shorter than the theoretical values by 33%, and that in the first survey was shorter by 66%. Because Eq. (10) does not consider vertical mixing due to tidal currents, which tends to prevent the offshore movement of a plume (Guo and Valle-Levinson, 2007), the longer predicted distance is understandable. Meanwhile, the difference between Eq. (10) and observations could also be caused by temporal variations in river discharge because Eq. (10) is based on a constant river discharge.

4.3. Dynamical examination on the variability of the plume with river discharge

The box model calculations in Section 3.3 demonstrated that the water exchange between the survey area and the area outside the sea is roughly proportional to the river discharge. For a dynamical interpretation, we calculated the geostrophic transport within the plume and the wind-driven transport across the lateral boundary of the survey area. The latter is considered as a representative ageostrophic transport.

Table 2
Calculation of offshore distance of the plume front based on the formula given by Yankovsky and Chapman (1997). B denotes width of river mouth and $\Delta\rho$ denotes density difference between plume water and ambient water; see Eq. (10) for meaning of other terms.

	B (km)	h_i (m)	v_i (m s^{-1})	$\Delta\rho$ (kg m^{-3})	ρ_0 (kg m^{-3})	y_s (km)	Observed offshore distance (km)
First survey	1	1	0.2	3.0	1019	9	3
Second survey	1	2	1.8	12.0	1019	46	>24[a]
Third survey	1	2	0.2	9.0	1018	20	14

[a] Because the plume front in the second survey was beyond survey region, the distance was assumed to be larger than 24 km.

The geostrophic transport (Q_g) within the plume follows the equation given by Fong and Geyer (2002) as follows:

$$Q_g = \frac{\Delta\rho g}{2\rho f}(h_0)^2 \tag{11}$$

where $\Delta\rho$ is the difference in density between the plume and ambient water, ρ is the density of ambient water (1020 kg m^{-3} for three surveys), g is gravity acceleration and h_0 is the plume thickness at the coast. Values of $\Delta\rho$ for the three surveys are shown in Table 3. According to Fig. 6g–i, h_0 was chosen to be 1.5, 5 and 2 m, respectively, corresponding to the 28-isohaline for the first survey and the 26-isohalines for the second and third surveys. The calculated Q_g values were 263, 7500 and 1022 m^3 s^{-1}, respectively. The ratios of Q_g to the corresponding river discharge were $\sim$2 in all three surveys. By assuming that this ratio was maintained throughout the survey periods and using the mean river discharge during the period between the first survey and the second survey and between the second survey and the third survey (Table 1), the mean values of Q_g for the two periods mentioned above were calculated as 4.46×10^8 and 2.04×10^8 m^3 day^{-1}.

The wind-induced outflow transport volume (V_E) across the lateral boundary of the survey area was calculated by

$$V_E = \sum_{i=1,5} \frac{\tau_i}{\rho f} L_i \tag{12}$$

where L_i is the distance between the farthest points of two neighbor sections and τ_i is the wind stress component parallel to L. The calculated V_E was 2.63×10^8 m^3 day^{-1} for the period between the first survey and the second survey and 2.87×10^8 m^3 day^{-1} for the period between the second survey and the third survey.

Combining this information with Table 1, the sum of the geostrophic transport and wind-driven transport can account for only 25–36% of the outflow flux from the survey area. Apparently, other processes are also important to the water exchange between the survey area and the area outside it. A full understanding of this problem requires the use of a numerical model.

Based on scaling analysis of the continuity and momentum equations, Garvine (1995) suggested using the Kelvin number (K) to categorize river plumes. The Kelvin number represents the ratio of the across-shore length of the plume to the baroclinic Rossby radius and is expressed as

$$K \equiv \frac{D}{c/f} \tag{13}$$

where D is the across-shore length (i.e., the observed offshore distance of the plume in Table 2), and c is the internal wave phase speed based on the difference in density between the plume and the ambient water.

Following Eq. (13), we obtained values of 0.6, 2.8 and 1.8 for the Kelvin numbers for the three surveys (Table 3). According to Garvine (1995), if the Kelvin number is less than 1, the advection term in the momentum equation is relatively strong while the Coriolis force is relatively weak, as in the small K-limiting case. If the Kelvin number is larger than 1, the advection term is weak and the Coriolis term strong, as in the large K-limiting case. Therefore, the values of the Kelvin numbers

Table 3
Calculation of geostrophic transport (Q_g) based on Eq. (11) and Kelvin number (K) based on Eq. (13). See Eqs. (11) and (13) for meaning of each term.

	$\Delta\rho$ (kg m^{-3})	h_0 (m)	Q_g (m^3 s^{-1})	K
First survey	2.2	1.5	263	0.56
Second survey	5.6	5	7500	2.8
Third survey	4.8	2	1022	1.8

from three surveys (Table 3) indicate that the plume dynamics were altered dramatically by the abrupt changes in Yellow River discharge during the water regulation event. From the surface salinity distribution (Fig. 3a, d and g), we can deduce that the bulge was weak or did not exist before the water regulation event, but became strong during and after the water regulation event. Accordingly, the Kelvin number may be considered as an indicator of the bulge state: the bulge is strong when the Kelvin number is relatively large and is weak when the Kelvin number is small.

5. Conclusions

In the three field surveys carried out before, during and after the water regulation event that occurred in the Yellow River in 2009, we observed the responses of a plume to an abrupt change in river discharge. The distribution of low salinity water was different between the surface layer and bottom layer. In the surface layer, low salinity water concentrated around the river mouth before the water regulation event. As a large amount of river water flowed into the sea during the water regulation event, the plume spread offshore with a quasi-symmetrical distribution in the direction of river water outflow. After the water regulation event, most of the diluted water was identified close to the river mouth and turned downstream in a Kelvin wave sense. Meanwhile, the plume in the bottom layer occupied a smaller area than that in the surface layer, and the diluted water was generally distributed in the downstream direction.

Box model analysis indicated that the water exchange rate between the water around the river mouth and the outside area was proportional to the river discharge. The geostrophic transport within the plume and the wind-driven transport across the lateral boundary of survey area can account for only 25–36% of the outflow flux from the survey area. A downward transport of freshwater through vertical mixing was evident during the observation period. A comparison of the stirring power due to tidal current and that due to surface winds suggested that the impact of wind mixing was comparable with that of tidal mixing in the area close to the river mouth and was dominant over offshore areas. The difference between the offshore spreading distance of the plume predicted by the equation based on a theoretical study and that observed in this study suggests that the inclusion of vertical mixing and the temporal variation in river discharge in future theoretical studies. The change in Kelvin number, from a value less than 1 before the water regulation event to a value larger than 1 during and after the event, suggests an alteration of the plume dynamics due to the abrupt change in river discharge. Because some parameters such as the vertical viscosity and tidal current data used in above analysis were from other studies, it is necessary to confirm them by using numerical modeling or direct observations in the future.

Acknowledgments

We are very grateful to all of the crews involved in the three surveys. We also thank Prof. Jing Zhang of East China Normal University and Prof. Wensheng Jiang of Ocean University of China for their kind help. We appreciate two reviewers for their critical comments that are very helpful to improve the manuscript. This study was funded by the Natural Science Foundation of China (No. 40706007), the Key Laboratory of Marine Environment and Ecology (Ocean University of China), Ministry of Education, and the State Key Laboratory of Estuarine and Coastal Research, East China Normal University (No. 200813). Xinyu Guo was supported by a Grant-in-Aid for the Global COE Program from the Ministry of Education, Culture, Sports, Science and Technology, Japan (MEXT) and the Japan Society for the Promotion of Science (JSPS) and JSPS KAKENHI (21310012).

References

Choi, B.J., Wilkin, J.L., 2007. The effect of wind on the dispersal of the Hudson River plume. Journal of Physical Oceanography 37, 1878–1897.
Fong, D.A., 1998. Dynamics of freshwater plumes: observations and numerical modeling of the wind-forced response and alongshore freshwater transport. Ph.D. Thesis, Joint Program in Oceanography, MIT/WHOI.
Fong, D.A., Geyer, W.R., 2002. The alongshore transport of freshwater in a surface-trapped river plume. Journal of Physical Oceanography 32, 957–972.
García Berdeal, I., Hickey, B.M., Kawase, M., 2002. Influence of wind stress and ambient flow on a high discharge river plume. Journal of Geophysical Research 107, 3130.
Garvine, R.W., 1995. A dynamical system for classifying buoyant coastal discharges. Continental Shelf Research 15, 1585–1596.
Gordon Jr, D.C., Boudreau, P.R., Mann, K.H., Ong, J.-E., Silvert, W.L., Smith S.V., Wattayakorn, G., Wulff, F., Yanagi, T., 1996. LOICZ Biogeochemical modelling guidelines. LOICZ Reports & studies, No. 5, pp. 1–96 〈http://www.nioz.nl/loicz/〉.
Guo, X.Y., Valle-Levinson, A., 2007. Tidal effects on estuarine circulation and outflow plume in the Chesapeake Bay. Continental Shelf Research 27, 20–42.
Isobe, A., 2005. Ballooning of river-plume bulge and its stabilization by tidal currents. Journal of Physical Oceanography 35, 2337–2351.
Kourafalou, V.H., 1999. Process studies on the Po River plume, North Adriatic Sea. Journal of Geophysical Research 104, 29963–29985.
Kourafalou, V.H., 2001. River plume development in semi-enclosed Mediterranean regions: North Adriatic Sea and Northwestern Aegean Sea. Journal of Marine Systems 30, 181–205.
Liu, F.Y., 1989. Observation of Yellow River plume and its frontal zone. Marine Science 5, 33–36 (in Chinese, with English abstract).
Mao, X.Y., Jiang, W.S., Zhao, P., Gao, H.W., 2008. A 3-D numerical study of salinity variations in the Bohai Sea during the recent years. Continental Shelf Research 28, 2689–2699.
Prandle, D., 1982. The vertical structure of tidal currents. Geophysical & Astrophysical Fluid Dynamics 22, 29–49.
Pullen, J.D., Allen, J.S., 2000. Modeling studies of the coastal circulation off northern California: shelf response to a major Eel River flood event. Continental Shelf Research 20, 2213–2238.
Qiao, L.L., Bao, X.W., Wu, D.X., 2006. Analysis of tidal currents of Bohai Sea in Summer. The Ocean Engineering 24, 45–52 (in Chinese, with English abstract).
Sheldon, J.E., Alber, M., 2006. The calculation of estuarine turnover times using freshwater fraction and tidal prism models: a critical evaluation. Estuaries and Coasts 29, 133–146.
Simpson, J.H., Bowers, D., 1981. Models of stratification and frontal movement in shelf seas. Deep-Sea Research 28A, 727–738.
Wang, H.J., Yang, Z.S., Bi, N.S., Li, H.D., 2005. Rapid shifts of the river plume pathway off the Huanghe (Yellow) River mouth in response to Water-Sediment Regulation Scheme in 2005. Chinese Science Bulletin 50, 2878–2884.
Wang, H.J., Yang, Z.S., Saito, Y., Liu, J.P., Sun, X.X., 2006. Interannual and seasonal variation of the Huanghe (Yellow River) water discharge over the past 50 years: connections to impacts from ENSO events and dams. Global and Planetary Change 50, 212–225.
Wang, Q., Guo, X.Y., Takeoka, H., 2008. Seasonal variations of the Yellow River plume in the Bohai Sea: a model study. Journal of Geophysical Research 113, C08046.
Wu, D.X., Mu, L., Li, Q., Bao, X., Wan, X.Q., 2004. Long-term variation characteristics of the salinity of the Bohai Sea and the probable leading factors. Progress in Natural Science 14, 191–195 in Chinese.
Xing, J., Davies, A.M., 2002. Influence of topographic features and along shelf flow upon the Ebro plume. Continental Shelf Research 22, 199–227.
Yan, J.Y., 1999. Estimation and analysis for air-sea fluxes of heat and moisture over the neighbouring seas of China. Quarterly Journal of Applied Meteorology 10 (1), 9–19 (in Chinese, with English abstract).
Yankovsky, A.E., Chapman, D.C., 1997. A simple theory for the fate of buoyant coastal discharges. Journal of Physical Oceanography 27, 1386–1401.
Yankovsky, A.E., Hickey, B.M., Münchow, A.K., 2001. Impact of variable inflow on the dynamics of a coastal plume. Journal of Geophysical Research 106, 19809–19824.
Zhao, B.R., Cao, D.M., Pan, H., Tu, D.Z., 1994. Characteristics of tidal mixing in the Yellow Sea and its effects on the boundary of the Yellow Sea cold water mass. Studia Marina Sinica 35, 1–10 (in Chinese, with English abstract).
Zhao, B.R., Cao, D.M., Li, W.F., Wang, Q.M., 2001. Tidal mixing characters and tidal fronts phenomenons in the Bohai Sea. Acta Oceanologica Sinica 23, 113–118 (in Chinese, with English abstract).
Zhao, P., Jiang, W.S., Mao, X.Y., Gao, H.W., Guo, X.Y., 2010. Salinity change and influencing factor in the Laizhou Bay from 2000–2005. Oceanologia et Limnologia Sinica 41, 12-23 (in Chinese, with English abstract).